Journal of Catalysis 428 (2023) 115074

Contents lists available at ScienceDirect

Journal of Catalysis

journal homepage: www.elsevier.com/locate/jcat

Mechanism of sustainable photocatalysis based on doped-titanium dioxide nanoparticles for UV to visible light induced PET-RAFT photo-polymerization

Valentina Bellotti [a,1], Chiara Daldossi [a,1], Daniele Perilli [a], Massimiliano D'Arienzo [a], Matus Stredansky [b], Cristiana Di Valentin [a,*], Roberto Simonutti [a,*]

[a] Dipartimento di Scienza dei Materiali, Università degli Studi di Milano-Bicocca, Via R. Cozzi, 53, 20125 Milano, Italy
[b] Istituto Officina dei Materiali-CNR Laboratorio TASC, Strada Statale 14, km 163.4, I-34012 Trieste, Italy

ARTICLE INFO

Keywords:
PET-RAFT
Controlled polymerization
Titanium dioxide
Photocatalysis
DFT

ABSTRACT

Heterogeneous catalysis is an essential aspect for actual industrialization of chemical processes. Here a TiO_2-based powder, typically used in photocatalysis, is exploited for the first time for visible-light-regulated Photoinduced Electron/Energy (PET)-reversible addition–fragmentation chain-transfer (RAFT). Titania is a non-toxic, low-cost, and heterogeneous catalyst that can offer several advantages in terms of sustainable polymerization and photocatalyst (PC) recovery. In this work, we aim not only at unraveling the mechanism of photopolymerization and the important interactions involved, but also at red-shifting the absorption region to achieve vis-light polymerization. The combination of the experimental investigation with Density Functional Theory (DFT) calculations provides new insights into the interactions between the chain transfer agents (CTAs) and the TiO_2 surface, unveiling their pivotal role on the reaction rate and polymerization control. Moreover, to shift the polymerization under the less energetic blue light, high-surface area N-doped TiO_2 nanoparticles are employed, avoiding the CTA degradation often observed with UV irradiation and increasing the overall sustainability of the process.

1. Introduction

The use of photocatalysts has only recently been combined with polymer chemistry to develop the synthesis of well-defined macromolecules. The control over the molecular weights, narrow dispersity (Đ), and complex molecular architecture has been achieved with the development of reversible-deactivation radical polymerization (RDRP) techniques [1], amongst which reversible addition-fragmentation chain-transfer polymerization (RAFT) [2,3] is a well-established controlled polymerization process, compatible with the use of a variety of monomers, reaction conditions, and functional groups [4]. In the last few years, the additional possibility to trigger polymerization [5] and, more recently, depolymerization [6,7], by an external stimulus has gained great interest. In particular, the use of light as an energy source for activation is extremely appealing since electromagnetic irradiation has intrinsic spatial and temporal control, low process costs, low environmental impact, and it can be easily modulated in intensity and wavelength. Moreover, light allows to perform the reaction in a situation where high temperatures, harsh reaction conditions, or deoxygenation would not be tolerated [8]. RAFT polymerization has evolved into a versatile and attractive technique thanks to the alternative activation of the RAFT agent (also called chain transfer agent, CTA) through a photoredox catalyst (PC) via photoinduced energy/electron transfer process (PET-RAFT) (Scheme 1). A wide variety of photocatalysts has been tested so far, varying from transition metal complexes [9,10] to naturally derived photoactive compounds [11–13], organic dyes [14,15], and more complex structures such as perovskite nanocrystals [16], quantum dots [17,18] and graphitic carbon nitride [19].

Titanium dioxide (TiO_2) is a non-toxic, highly stable, cheap semiconducting metal oxide with outstanding photocatalytic properties. The photoactivity of TiO_2 was discovered in the 1930 s [20] and since then it has become one of the most widely used heterogeneous photocatalysts. Its applications range from the removal of pollutants and biological contaminants [21], to solar cell [22], and water splitting [23]. The major drawback of TiO_2 photocatalyst is its large bandgap corresponding to a value of 3.20 eV for bulk anatase and 3.02 eV for rutile

* Corresponding authors.
E-mail addresses: cristiana.divalentin@unimib.it (C. Di Valentin), roberto.simonutti@unimib.it (R. Simonutti).
[1] These authors contributed equally.

https://doi.org/10.1016/j.jcat.2023.07.015
Received 20 April 2023; Received in revised form 3 July 2023; Accepted 18 July 2023
Available online 20 July 2023

phase, i.e. the photocatalytic activity is triggered upon exposure to ultraviolet (UV) light. When photons with higher or equal energy to the TiO_2 bandgap (E_g) are absorbed, conduction-band (CB) electrons (e^-) and valence-band (VB) holes (h^+) are generated. However, about 90% of the photogenerated electron–hole pairs rapidly recombine after the separation, following both radiative and nonradiative pathways [24–26]. The poor light absorption and charge separation under visible light irradiation limit the application of TiO_2 in various fields where solar energy is exploited as renewable energy source. For this reason, considerable effort has been made to improve the absorption of TiO_2 in the visible part of the electromagnetic spectrum. The most common strategies include the band gap engineering by the introduction of impurities [27–30], or the surface functionalization with molecules, such as organic dyes that are sensitive to visible light [31,32]. Among various methodologies, nitrogen-doped TiO_2 (N-doped TiO_2) was found to produce photocatalytic activity under visible light irradiation [33–38].

You and co-workers investigated the possible use of TiO_2 as a photocatalyst for PET-RAFT [39]. In their work, PMMA was synthesized in a controlled manner using Degussa P25 titanium dioxide nanoparticles (TiO_2 NPs) under UV irradiation. Control of the reaction was lost after 4 h, and low monomer conversion was reached. 4-cyanopentanoic acid dithiobenzoate (CPADB) was selected as the chain transfer agent because its redox potential is greater than the redox potential of TiO_2, which allows the CTA to be reduced *via* the PET process initiating the polymerization. An electron transfer pathway was proposed [39], but no experimental evidence of the mechanism has been provided so far.

Although the RAFT polymerization is a well-known process, when electromagnetic irradiation is used to activate the CTA, the reaction mechanism becomes unclear, because the latter acts as both the chain transfer agent, as in the common RAFT protocol, and the initiating species. Light irradiation can directly excite the CTA that undergoes homolytic fragmentation followed by initiation of radical reactions. This photoinduced homolysis process is known as photoiniferter (PI) mechanism [40], and occurs when the electromagnetic irradiation provides enough energy to break the C-S bond, often causing the irreversible photolysis and degradation of the CTA [41–43]. The introduction of a photoredox catalyst, as in PET-RAFT, allows the use of the whole ultraviolet, visible, and infrared spectrum depending on the PC nature. In these cases, it was proposed [44,45] that the pivotal step for the generation of the initiating radical species involves a photoinduced electron or energy transfer from the excited state photoredox catalyst to the CTA, which becomes able to directly initiate the polymerization.

Despite the potential advantages of TiO_2 in terms of cost, toxicity, recyclability, and easiness of manipulation, the use of this material in polymerization is still limited. In the present contribution, our aim is to provide the reader with a comprehensive study of the photocatalytic mechanism of PET-RAFT polymerization using commercial Degussa P25 TiO_2 and synthetized N-TiO_2 nanoparticles. Two dithiobenzoates have been selected for this study among the mostly used CTAs for the polymerization of methacrylates and methacrylamides: 4-cyanopentanoic acid dithiobenzoate (CPADB) and 2-cyanoisopropyl dithiobenzoate (CPDB). These were reported to provide good control over molecular weight, dispersity, and end-group fidelity in the traditional RAFT [46,47]. We have combined experiments with first-principles calculations, based on a hybrid density functional theory (DFT) method, to determine the steps that lead to the initiation of the PET-RAFT process and to rationalize the underlying reasons why CPADB is more efficient than CPDB. Using this insight, we also optimized the experimental setup of synthesis by enlarging the NP surface area and by introducing nitrogen dopants. Indeed, N-TiO_2 nanoparticles could harvest lower energy light (460 nm) in the visible range leading also to better control and an enhanced degree of livingness of the polymerization process. Therefore, our study, besides highlighting the promising application of titania in PET-RAFT polymerization, provides specific hints for a better design and optimization of the procedure.

2. Experimental section

2.1. Materials

Dichloromethane (DCM), methanol (MeOH), N,N'-dimethylformamide (DMF), tetrahydrofuran (THF), deuterated chloroform ($CDCl_3$) were purchased from Sigma Aldrich and used as received. Methyl methacrylate (MMA) was purchased from Sigma and purified in basic alumina column before use to remove the inhibitor. 4-dimethylaminopyridine (DMAP) and 2-cyanoisopropyl dithiobenzoate (CPDB) was purchased from Sigma Aldrich whereas 4-cyanopentanoic acid dithiobenzoate (CPADB) was synthetized as reported in literature [48,49] starting from 4,4′-azobis(4-cyanopentanoic acid) and bis(thiobenzoyl) disulfide, both purchased by Sigma Aldrich. Degussa P25 titanium dioxide (TiO_2) powder (78% anatase, 14% rutile and the remaining 8% amorphous phase) [48] with a primary particle diameter of 30 nm and BET surface area of 50 m^2/g, was purchased by Evonik TiO_2. N-TiO_2 was synthesized according to literature [51] starting from titanium butoxide, $Ti(OBu)_4$, and diethanolamine (DEA) purchased by Sigma Aldrich.

The LED UV light source used was UV Z5 High Power series (CUN66A1G) with a peak wavelength $\lambda = 367 \pm 3$ nm and a radiant flux $\Phi e = 1.85$ W assembled on a het sink. Blue LED light ($\lambda = 460$ nm) was purchased in strips and accommodate in circular shape in a home-made photoreactor with a light intensity of 10 mW/cm^2.

2.2. Synthetic procedures

2.2.1. Synthesis of CPADB chain transfer agent

Synthesis of 4-cyanopentanoic acid dithiobenzoate (CPADB) was performed according to literature [49,50]. 4,4′-azobis(4-cyanopentanoic acid) (2.94 g, 10.5 mmol) and bis(thiobenzoyl) disulfide (DTBA) (2.15 g, 7 mmol) were dissolved in distilled ethyl acetate (40 mL) and heated at reflux for 18 h. After removal of solvent in vacuum, the crude product was isolated by column chromatography using ethyl acetate:n-hexane 2:3 as eluent. The red fraction was collected and dried out under vacuum to afford 4-cyano-4-((thiobenzoyl)sulfanyl)pentanoic as a red oil. This latter product was placed in freezer at −20 °C to crystallize. The compound was recrystallized from ethyl acetate:n-hexane 2:3 and analysed through NMR and FT-IR spectroscopy; yield was 50.1%.

2.2.2. Grafting of CPADB on TiO_2 surface

TiO_2 (1 g) and CPADB (50, 34 and 10 wt/wt) were added to a 50 mL two neck round-bottom flask thermal pretreated. The system was left under vacuum for 2 h in order to remove any trace of water and it was suspended, under anhydrous conditions, in 10 mL DMF (0.1 g/mL in all cases). The suspension was sonicated for 20 min and kept for 96 h in the dark under stirring at room temperature in an inert nitrogen atmosphere. The grafted TiO_2 particles (TiO_2@CPADB) were recovered by

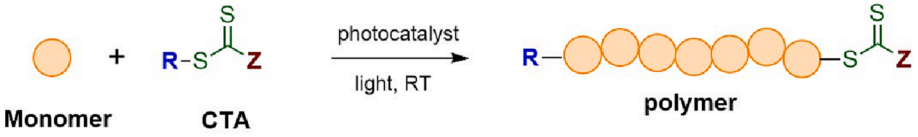

Scheme 1. General scheme for PET-RAFT polymerization. The newly formed polymer chain is inserted between the R and ZSS groups after the cleavage of the C-S bond in presence of the photocatalyst under light irradiation.

centrifugation (30 min at 6000 rpm), removing the supernatant which contained the residual unreacted CTA. The powder was washed twice for 30 min with ethyl acetate and twice with CH_2Cl_2. The result powder was dried under vacuum overnight to remove the residual solvent. DLS, IR, TGA and elementary analysis (Table 1) were performed to analyze the degree of functionalization.

2.2.3. General procedure for the kinetic studies of PET-RAFT polymerization of MMA with CPDB and CPADB chain transfer agents

A stock dispersion of Degussa P25 TiO_2 in DMF was prepared with a concentration of photocatalyst equal to 0.32 mg/mL; before each polymerization the stock dispersion was sonicated for 30 min in order to finely disperse the nanoparticles. Two different chain transfer agents were tested: CPADB and CPDB. In the first case, MMA (5.75 g, 57.48 mmol) and CPADB (53.5 mg, 0.19 mmol), with a ratio of [MMA]:[CPADB] = 300:1 was added to a 50 mL Schlenk tube together with 2.5 mL of TiO_2 dispersion [MMA] = 6.67 M. In the second case, MMA (14.39 g, 143.7 mmol) and CPDB (106.0 mg, 0.48 mmol), with a ratio of [MMA]:[CPDB] = 300:1 was added to a 50 mL Schlenk tube together with 5 mL of TiO_2 dispersion [MMA] = 7.08 M. For the experiment with the addition of DMAP as sacrificial electron donor a ratio of [CTA]:[DMAP] = 1:5 was used. After four freeze–thaw-pump cycles the tube was filled with nitrogen, closed in a dark box with reflecting walls and irradiated under UV LED light. The instant in which the light source is turned on is considered the polymerization initial time (t_0). Polymerization reactions were quenched in an ice bath at selected times. The TiO_2 nanoparticles were recovered by centrifugation (15 min at 6000 rpm) and the supernatant was precipitated in a large excess of cold methanol. NMR was used for determinate M_n and conversion, GPC with St standard displayed the Mn and dispersity. The titanium dioxide powder was washed three times and the residual solvent evaporated under vacuum overnight for TGA analysis.

2.2.4. Increasing titanium dioxide concentrations and surface area

Different concentrations of TiO_2 were employed and the solvent to monomer ratio was varied to obtain various degree of agglomeration, and consequently different surface area of the photocatalyst. A stock dispersion of Degussa P25 TiO_2 in DMF was prepared with a concentration of photocatalyst equal to 5 mg/mL and sonicated for 30 min. Selected volumes of the dispersion were withdrawn and added to the DMF/MMA mixture with a DMF volume fraction respect to the monomer of 0.23 for the 0.15 mg/mL final TiO_2 concentration experiment, 0.11 for 0.168 mg/mL, 0.07 for 0.174 mg/mL and 0.71 for 0.32, 0.48, 1.28, 1.92, 3.20 mg/mL. All the reaction mixtures were analyzed by DLS to obtain the hydrodynamic volume of the photocatalyst aggregates in solution and then the CTA added to the mixture. The polymerization procedure is the same as described above. The ratio [MMA]:[CPDB] was maintained constant to 300:1 and all the reactions stopped after 4 h.

2.2.5. Synthesis and characterization of of N-doped TiO_2

N-doped TiO_2 was prepared by a modified literature procedure [51]. $Ti(OBu)_4$ (2.17 mg, 0.063 mmol) was added to a mixture of 8.75 mL of EtOH and diethanolamine (DEA) (1.31 g, 0.0125 mol) and stirred at room temperature. After 2 h, the solution was hydrolyzed by the addition of 230 μL of water and stirred for another 2 h. The final product was precipitated in acetone, recovered by centrifugation (10 min at 6000 rpm) and dried overnight. Finally, the powder was calcined in air at 550 °C for 1 h.

The crystal phases of the final product were characterized by powder X-ray diffraction, Raman spectrometer and TEM. Diffuse reflectance spectroscopy was performed using a UV/vis/NIR spectrophotometer. The reflectance was transformed by the Kubelka-Munk (K-M or F(R)) method which is based on the following equation:

$$F(R) = \frac{(1-R)^2}{2R} \approx a \quad (1)$$

where R is the reflectance and F(R) is proportional to the extinction coefficient (α). The determination of the optical energy gap (E_g) is possible by plotting the $(F(R) \times E)^{1/2}$ versus E and fitting the linear portion of the curve by a straight line. The x-axis intersection, calculated by dividing the intercept by the slope, provides the value for E_g [52]. Using this methodology, a shift of 0.3 eV, i.e. from 3.1 eV to 2.8 eV (438 nm) was determined. Finally, the presence of nitrogen into the synthetized N-TiO_2 structure was investigated using Electron Paramagnetic Resonance (EPR) and X-Ray Photoelectron Spectroscopy (XPS).

2.2.6. PET-RAFT polymerization of MMA with CPDB and CPADB chain transfer agent using N-doped titanium dioxide

3.08 mg of N-TiO_2 previously synthetized were dispersed in 4.59 mL of DMF and sonicated for 30 min. MMA (1.73 g, 17.24 mmol), CPADB (16.05 mg, 0.057 mmol) or CPDB (12.72 mg, 0.057 mmol) were added to the dispersion. The final concentration of N-doped titanium dioxide was 0.48 mg/mL. After four freeze–thaw-pump cycles the tube was filled with nitrogen and closed in a dark box with reflecting walls and irradiated under blue LED light. Polymerization reactions were quenched in ice bath and stored in the dark. The N-TiO_2 nanoparticles were recovered by centrifugation (15 min at 6000 rpm) and the supernatant was precipitated in a large excess of cold methanol. NMR was used for determinate Mn and conversion, GPC with St standard displayed the Mn and dispersity.

2.3. Computational methods

Considering the size of the Degussa P25 nanoparticles used experimentally, we chose to model the TiO_2 surface using a periodic slab model. In fact, the effect of the curvature of the surface can be considered negligible when the radius of the nanoparticles is sufficiently large, as it is in our experimental setup (Z-average diameter of 263 (±0.34) nm from the DLS analysis as reported in **Section 3.1**). Degussa P25 nanoparticles contain both anatase and rutile TiO_2 phases in a ratio of about 3:1, and anatase is usually considered to be more suitable for photocatalytic applications with respect to rutile because of its indirect band gap of 3.20 eV, which is higher than for rutile (3.02 eV), making the recombination of photogenerated charge carriers slower. For these reasons, we chose to model an anatase surface and, specifically, the anatase (1 0 1) TiO_2 surface since it is known to be the most stable and the most widely exposed.

All DFT calculations were performed with the CRYSTAL17 [53] package where the Kohn-Sham orbitals are expanded in Gaussian type orbitals. The all-electron basis sets are Ti 86–411(d41) and O 8–411(d1) for the atoms of TiO_2; H 511(p1), C 6–311(d11), N 7–311(d1), O 8–411 (d11) and S 86–3111(d11) for the atoms of the CTAs. The B3LYP hybrid functional [54], corrected with the Grimme's approach (B3LYP-D*) [55,56] to include dispersion forces, has been used throughout this work in order to correctly describe the electronic structure of anatase TiO_2.

The anatase (1 0 1) TiO_2 surface was modelled using a periodic slab of 4 × 2 supercell (a = 15.1575 Å, b = 11.1457 Å) with three triatomic layers for a total of 144 atoms. The periodicity was considered along the [1 0 1] and [0 1 0] directions while no periodic boundary conditions were imposed in the direction perpendicular to the surface. The supercell model is useful to control the coverage of the surface. For this study, the obtained coverage is 0.006 molecule/Å^2. The calculations were performed sampling the Γ point only in the first Brillouin zone. The lowest lying row of Ti and O atoms of the bottom layer were kept fixed at the optimized bulk positions during the geometry optimization.

Cutoff limits in the evaluation of Coulomb and exchange series/sums appearing in the SCF equation were set to 10^{-7} for Coulomb overlap tolerance, 10^{-7} for Coulomb penetration tolerance, 10^{-7} for exchange overlap tolerance, 10^{-7} for exchange pseudo-overlap in the direct space, and 10^{-14} for exchange pseudo-overlap in the reciprocal space. The condition for the SCF convergence was set to 10^{-6} hartree on the total

energy difference between two subsequent cycles. Convergence in the geometry optimization process is tested on the root-mean-square (RMS) and the absolute value of the largest component of both the gradients and nuclear displacements. The default thresholds for geometry optimization within the CRYSTAL code have been used for all atoms: maximum and RMS forces have been set to 4.50×10^{-4} and 3.0×10^{-4} a.u., and maximum and RMS atomic displacements to 1.80×10^{-3} and 1.20×10^{-3} a.u., respectively.

The density of states (DOS) and projected density of states (PDOS) were computed using a $30 \times 30 \times 1$ k-point mesh, setting the zero energy to the vacuum level.

3. Results and discussion

Following the preliminary work of You and co-workers [39], the kinetics of PMMA polymerization was conducted using the two different CTAs and the results are reported in **Section 3.1**. Given the interesting kinetic behaviors of the two CTAs, we investigated the systems also by computational means, to obtain a deeper understanding of such experimental results and determine the underlying of the three possible mechanisms (Scheme 2). In **Section 3.2** we present the computational analysis of CTAs' adsorption configurations along with their structural and electronic properties resulting from hybrid DFT calculations (B3LYP-D*). This analysis was aimed to understand which mechanism is involved in the initiating PET process and it has been experimentally validated in **Section 3.3** using electron donating amines. In **Section 3.4** we discuss further calculations on the CTAs' fragments adsorption at the TiO_2 surface revealing the presence of competitive interactions. To empirically support these computational observations, in **Section 3.5** polymerization was repeated at different catalyst concentrations, meaning different agglomeration states and consequently, different surface areas, and additional kinetic studies were performed. Finally, **Section 3.6** is focused on the development of N-doped titanium dioxide nanoparticles able to drive the polymerization under visible irradiation. In the following sections, to distinguish between the different titanium dioxide-based compounds we use "TiO_2" to refer to Degussa P25 TiO_2 nanoparticles, "TiO_2@CPADB" to refer to TiO_2 grafted with CPADB, and "N-TiO_2" to refer to synthetized N-doped TiO_2 nanoparticles.

3.1. Kinetic studies with different CTAs

PET-RAFT polymerization of PMMA using TiO_2 as a photocatalyst (PC) under UV light ($\lambda = 356$ nm) at room temperature was performed with two chain transfer agents: CPDB and CPADB. DMF was chosen as reaction medium since polar solvents are more suitable for TiO_2 catalysts as they can stabilize the charge-separated species, which may facilitate the initiation of the reaction. In addition, the TiO_2 surface is covered by hydroxyl functionalities [57,58], which are better stabilized in a polar environment. The DLS analysis results in a Z-average diameter of 263 (±0.34) nm, highlighting the efficiency of this solvent to disperse the chosen photocatalyst (**Fig. S1**). PET-RAFT polymerization using both CPADB and CPDB was performed and the kinetics of the process was analyzed. Monomer conversion was calculated through NMR analysis (**Fig. S2**).

As shown in Fig. 1 the polymerization with CPADB is faster than the one with CPDB. We believe that this trend can be explained by the additional interaction of the –COOH terminal group of CPADB with the surface of the nanoparticles, as well as the proximity of CTA to the photocatalyst surface that facilitates the PET process and consequently the reaction rate. Although the polymerization rate increases in the case of CPADB, the closeness to the TiO_2 photocatalyst seems to negatively affect the livingness of the polymeric chains. In fact, during the polymerization the red dispersion turns into white, suggesting higher degradation of the CTA chain-termini. High monomer conversion or long irradiation time have been proposed to increase the UV photolysis of the CTA, leading to partial dithioester degradation [43]. In fact, the value of dispersity of the polymer obtained with CPADB increases over time reaching a value of $Đ = 1.57$ after 4 h and $Đ = 1.9$ after 5 h. In contrast, in the presence of CPDB a higher control of the polymerization is attained, with $Đ = 1.32$ after reaction time of 5 h (**Table S1**). No polymerization was observed in the absence of the CTAs and light, whereas PMMA was rapidly polymerized under UV irradiation without the PC (**Table S1**), but with a very high dispersity ($Đ > 2.5$) and non-symmetric molecular weight distribution (**Fig. S3**), which is typical of non-controlled free radical polymerization. In this case, the high energetic light can activate the CTA's C-S bond starting a photoiniferter mechanism (Scheme 2**a**), which quickly results in a loss of polymerization control. Accordingly, UV photolysis of the RAFT agent has been reported in literature [42,59] and results in unavoidable loss of the living character due to unspecified side reactions. In summary, these experiments confirm that the PET-RAFT protocol needs both light and CTA to successfully obtain the polymer in a controlled manner, as typical of RDRP techniques.

3.1.1. Interaction between CPADB and TiO_2 surface

The CPADB chain transfer agent is characterized by a carboxylic-acid end functionality, suitable for the grafting onto the TiO_2 surface through strong Ti-O bonds (**Fig. S4**) [60–62]. The anchoring ability of the carboxylic group is well-known and amply exploited in the development of dye sensitized solar cells and other photocatalyst.

To this aim, various suspensions of CPADB and TiO_2 in DMF were prepared and kept for 96 h in the dark under stirring at room temperature. Grafting of CPADB to TiO_2 surface (TiO_2@CPADB) at different coverage density was confirmed by elementary analysis (Table 1), IR, and TGA (Fig. 2). Out of the three samples investigated, in Fig. 2 we report the IR and TGA of sample TiO_2@CPADB_50 alone, since all of them show the same trends.

The characteristic C = O vibration mode, of the free aliphatic acids, at 1700 cm^{-1} is absent whereas it can be noticed the presence of both asymmetric and symmetric stretching bands of the carboxyl moiety (COO^-), respectively at 1660 and 1437 cm^{-1}, which confirm the chelating or bridging bidentate coordination between titanium oxide and the carboxylic group. In addition, sp^3 C–H stretching vibrations at 2967 and 2935 cm^{-1} can be attributed to the aliphatic CPADB chain,

Table 1
Data of CPADB grafting on TiO_2 (TiO_2@CPADB).

Entry	TiO_2/CPADB (wt/wt)	[TiO_2] (g/mL)	CPADB Covering NP [a] (wt/wt%)	Σ [b] (molecules/nm^2)	D (nm)
TiO_2@CPADB_50	50	0.1	1.7 ± 0.1	0.78	1.28
TiO_2@CPADB_34	34	0.1	2.1 ± 0.1	0.92	1.17
TiO_2@CPADB_10	10	0.1	2.7 ± 0.4	1.03	1.11

[a] Average between TGA and CHNS analysis.

[b] Calculated through the following formula:. $\Sigma = \dfrac{\left(\dfrac{mol\,CPADB}{g\,TiO_2}\right) \bullet N_A[ch/mol]}{A_{sup}TiO_2\,[m^2/g] \bullet 10^{18}\,[nm^2/m^2]}$

while aromatic sp^2 stretching mode is probably covered by the –OH group stretching vibrations of physisorbed moisture.

The same protocol has been conducted for CPDB but no significant adsorption has been obtained. These results are in good agreement with the optimized geometry of the CPADB adsorbed on the TiO_2 (1 0 1) anatase surface retrieved by computational studies, showing bridging bidentate coordination (see **Section 3.2**).

Having demonstrated the interaction between CPADB and TiO_2, we decided to follow the same characterization protocol to demonstrate that this interaction occurs likewise during polymerization under irradiation. At the end of the PET-RAFT polymerization, the crude reaction mixture was centrifuged to recover the heterogeneous photocatalyst. After four washing cycles, the FT-ATR spectrum of the treated powder (Fig. 2**a**), showed the characteristic PMMA signals, i.e. the peaks at 1721 cm^{-1} (C = O), 1147 cm^{-1} (C-O-C) and 1435 cm^{-1} (C–H stretching vibrations of the –CH_3 and –CH_2- groups). The amount of grafted polymer was quantitatively assessed by TGA analysis, resulting in 3 wt% (Fig. 2**b**).

3.2. Computational investigation of the initiating PET mechanism

A computational DFT study was conducted on all three potential mechanisms of PET-RAFT polymerization. In the photoiniferter process (Scheme 2**a**), the light irradiation directly excites the CTA leading to the fragmentation of the C-S bond and the formation of the two radical species: the radical initiator (R) and the thiocarbonyl radical (ZSS). The energy required to homolytically break the C-S bond ($E_{C\text{-}S}$) has been calculated using the following equation:

$$E_{C-S} = E_R + E_{ZSS} - E_{CTA} \quad (2)$$

Where E_R is the energy of the thiocarbonyl radical, E_{ZSS} is the energy of

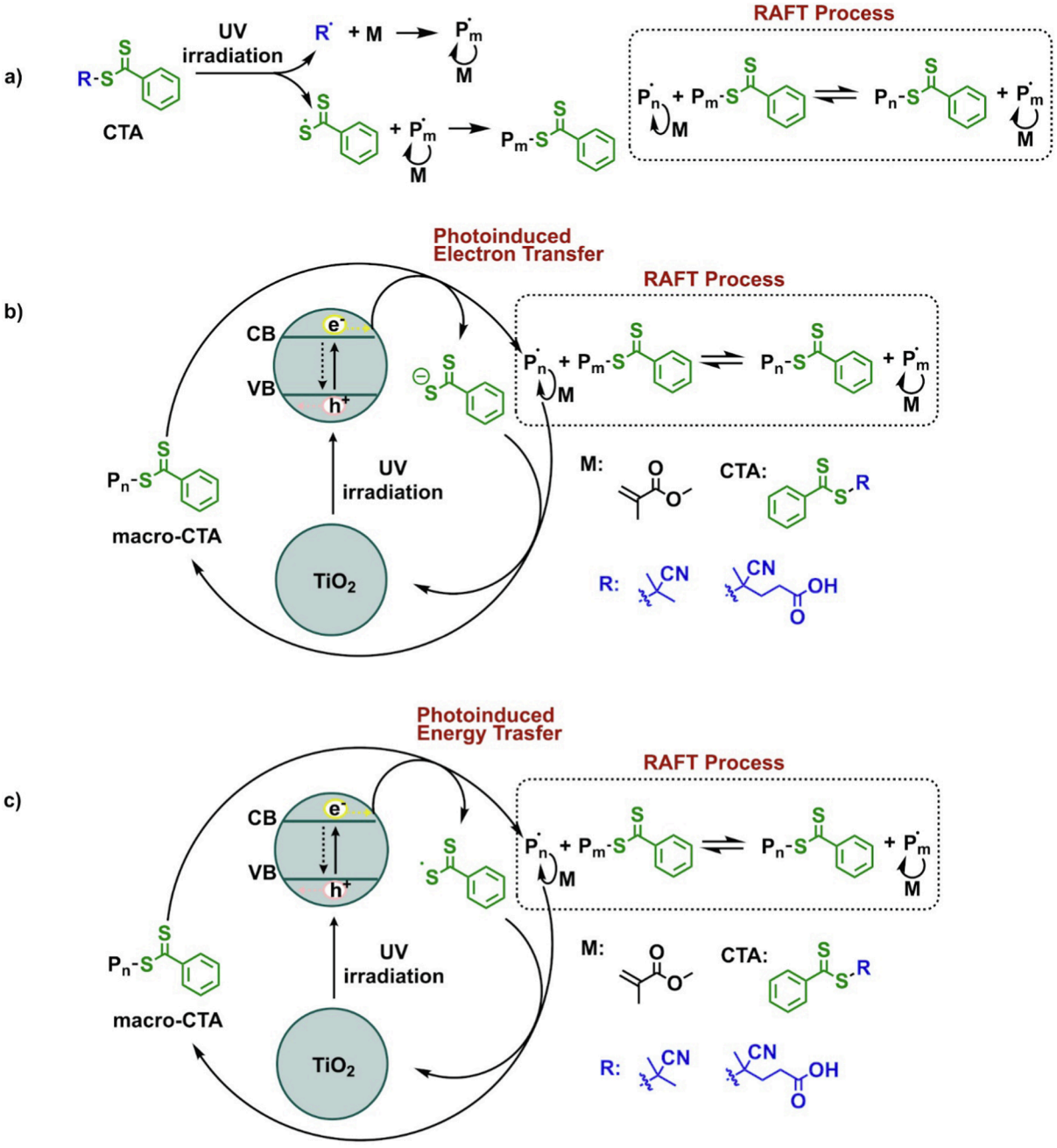

Scheme 2. Possible mechanisms of radical species generation: light-mediated pathway by a) photoiniferter process, or photocatalyst-mediated pathway by b) electron transfer mechanism or c) energy transfer mechanism.

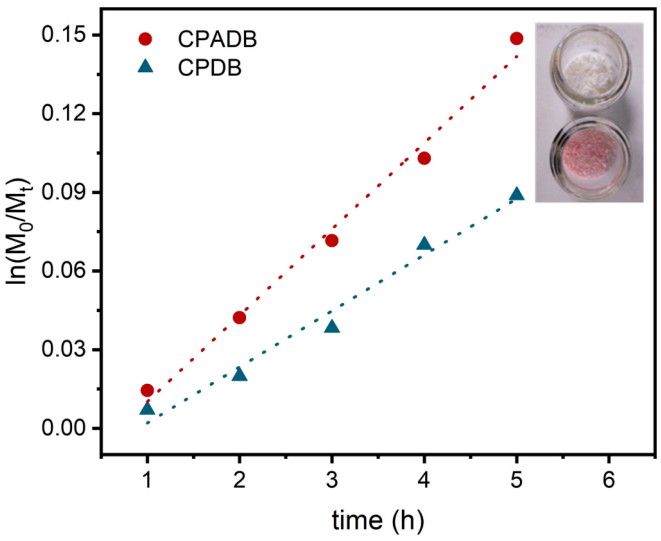

Fig. 1. Kinetic comparison of PMMA PET-RAFT polymerization using CPADB (red dots) and CPDB (green triangles) as CTAs under UV light irradiation with TiO_2 photocatalyst. Result refers to polymer content in solution (supernatant). The picture shows the final color of the resulting purified polymers after a reaction time of 5 h. (For interpretation of the references to color in this figure legend, the reader is referred to the web version of this article.)

the thiocarbonyl radical, and E_{CTA} is the energy of the chain transfer agent. For CPDB and CPADB, the calculated energy needed to homolytically break the C-S bond is 1.62 eV and 1.58 eV, respectively. Since the UV light source required to excite pristine TiO_2 (3.20 eV) can directly provide enough energy to fragment the C-S bond and form the two radicals without the need for the semiconductor to act as a photocatalyst, there is a serious possibility that the PET-RAFT process goes through a photoiniferter mechanism. This hypothesis has been experimentally proven to be a valid possibility through the control test experiment, where the polymerization was observed to occur in the presence of CTA and UV irradiation even in the absence of the TiO_2 photocatalyst (**Section 3.1**). However, we can safely exclude that this is the main reaction path at play in the presence of the PC because it would lead to a non-controlled polymerization (as shown in **Section 3.6**).

Differently, the first step of both the energy and electron transfer process involves the excitation of the photocatalyst, followed by the interaction between the photocatalyst in the excited state and the CTA leading to its fragmentation. In the case of an electron transfer (Scheme 2**b**), the excited electron of the photocatalyst is transferred to the CTA, occupying one of its first unoccupied orbitals. If the transferred electron goes into an empty state of the molecule with a non-bonding orbital distribution, then the CTA could favorably fragment into a radical initiator and a charged thiocarbonyl species. In the case of an energy transfer (Scheme 2**c**), the excitation energy required by the photocatalyst gets transferred to the CTA via either a Dexter or a Förster mechanism, both leading to the same final state, which is the excited CTA. After CTA excitation, homolytic fragmentation of the molecule can occur with the formation of the two radical species: the radical initiator and the thiocarbonyl radical.

To model these two mechanisms, we reproduced the adsorption of the two CTAs on TiO_2 (1 0 1) anatase surface. The adsorption energy (E_{ads}) of the CTAs on the TiO_2 (1 0 1) anatase surface model has been calculated as the difference between the total energy of the TiO_2/CTA system (E_{tot}) and the energy of the CTA (E_{CTA}) and that of the optimized TiO_2 surface slab model (E_{TiO2}):

$$E_{ads} = E_{tot} - (E_{CTA} + E_{TiO_2}) \quad (3)$$

CPDB optimized in the gas phase can interact and bind to the TiO_2 surface by the nitro and/or the sulfur group, for this reason, different adsorption modes have been considered: monoS, monoN, and bidentate (**Fig. S5**). The calculated adsorption energies are −0.94 eV, −1.14 eV, and −1.34 eV, respectively; thus, the bidentate configuration resulted to be the most stable. The bidentate is obtained through the interaction of the cyano and the sulfur groups of the CPDB with two undercoordinated (five-fold coordinated) Ti_{5c} of the anatase (1 0 1) surface.

CPADB, with respect to the CPDB molecule, presents an additional carboxylic group that is known to stably bind to the TiO_2 (1 0 1) anatase surface. The most favorable binding mode is a dissociated bridging bidentate way [12], with the two oxygen atoms of the carboxylic group (one of which is deprotonated with the proton migrating to a surface O atom) bonding with two undercoordinated Ti_{5c} atoms. Moreover, the aliphatic chain of the molecule bends towards the anatase surface to form another interaction between the cyano group and another Ti_{5c} atom of the surface (**Fig. S5**). The calculated adsorption energy for CPADB on the TiO_2 anatase surface is −1.93 eV, higher than those calculated for the CPDB, see above, due to the strong interaction of the carboxylic group with the surface that we have just described.

For the most stable adsorption configurations of CPDB and CPADB, we investigated the electronic properties through the total (TDOS) and the projected density of states (PDOS), as shown in Fig. 3.

As one should expect for the bare anatase surface, the states at the

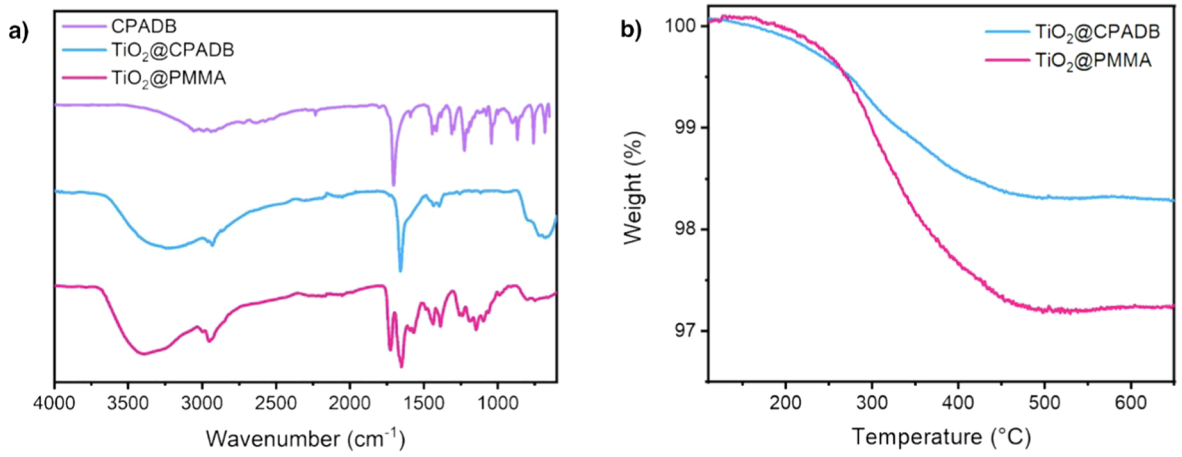

Fig. 2. a) FT-ATR of TiO_2 grafted with CPADB (blue line) and of TiO_2 at the end of PET-RAFT polymerization (pink line) in comparison with the spectrum of CPADB (purple line). b) TGA analysis of TiO_2 grafted with CPADB (blue line) and of TiO_2 at the end of PET-RAFT polymerization (pink line). The net weight loss percentage between 100° C and 650° C was assigned to the organic material degradation. (For interpretation of the references to color in this figure legend, the reader is referred to the web version of this article.)

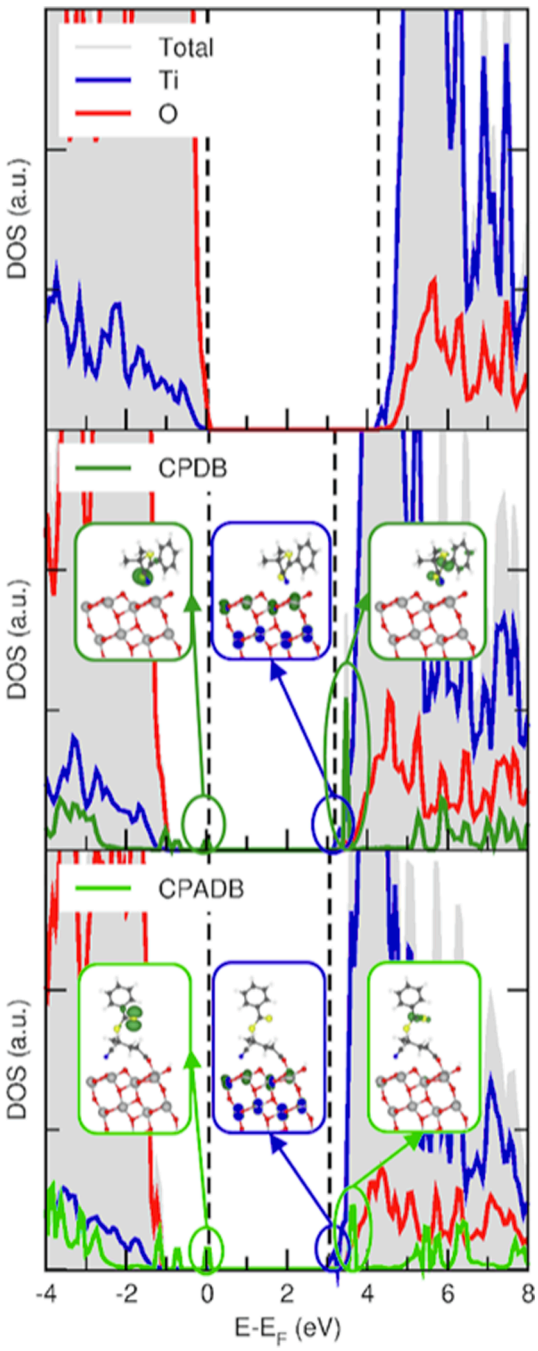

Fig. 3. TDOS and PDOS of the TiO_2 (1 0 1) anatase surface pristine (upper panel) and functionalized with CPDB (middle panel) and CPADB (lower panel). On each panel are reported the highest occupied state and the lowest unoccupied state using dashed lines, and the plotted density of the HOMO and LUMO molecular state and the lowest unoccupied state of the material.

top of the valence band are mainly composed of the O 2p contribution, while the states at the bottom of the conduction band are mainly composed of Ti 3d contribution. The calculated band gap of the material with the present setup and slab model is 4.25 eV. From the PDOS analysis of adsorbed CPDB and CPADB, there are molecular levels inside the band gap of the material that are occupied and, thus, reduce the gap between the highest occupied state and the lowest unoccupied state to 3.13 and 3.00 eV, respectively. These new states inside the band gap of TiO_2 correspond to π orbitals localized on one or both the S atoms of the CTAs, as shown in the plotted electronic density of Fig. 3. For both CTAs, the bottom of the conduction band of the system is still mainly composed of Ti atoms, while the first molecular empty states are localized inside the conduction band.

To justify the fragmentation of the CTA via an electron transfer mechanism, there should be an empty molecular state at the bottom of the conduction band characterized by a non-bonding orbital distribution on the C-S bond to be broken. The excited electron from the excited state of the TiO_2 could populate that non-bonding state leading to the molecule's fragmentation. However, no such state is observed in both the PDOS of CPDB and CPADB adsorbed on the TiO_2 (1 0 1) anatase surface. In fact, the LUMO of the molecule (shown in the plotted electronic density of Fig. 3) is not characterized by a distribution of the C-S bond, while the first empty state characterized by a non-bonding orbital distribution on the C-S bond to be broken is located deep inside the conduction band. These observations exclude the possibility of a polymerization initiated by an electron transfer mechanism of photoinduction.

On the other hand, an energy transfer mechanism of photoinduction is still plausible since the wide band gap offers enough energy to homolytically break the C-S bond, whose $E_{C\text{-}S}$ calculated is 1.62 eV and 1.58 eV for CPDB and CPADB, respectively as presented above. Therefore, we propose that CTA fragmentation takes place upon an energy transfer mechanism.

3.3. Experimental evidence of energy transfer mechanism

The hypothesis of an energy transfer mechanism has been experimentally supported by the use of sacrificial electron donors, i.e. amines. In fact, it has been demonstrated in PET-RAFT polymerization using Eosin Y [63] and cadmium selenide quantum dots [17] as photocatalysts, that tertiary amines (R_3N) can donate electrons to neutralize the photogenerated hole leading to formation of amine radical cations ($R_3N^{\bullet+}$). Thus, the use of tertiary amines is found to prevent photoexcited electron-hole recombination processes, improving the photoexcited electron lifetime and the catalyst turnover, but it has never been exploited in the case of TiO_2 catalyzed PET-RAFT.

Based on this, we decided to repeat the polymerization reactions in the presence of 4-dimethylaminopyridine (DMAP) as a sacrificial electron donor with a ratio of [CTA]:[DMAP] = 1:5. If the mechanism proceeds through an electron transfer, we expect that the presence of the amines results in an increase in the polymerization rate. However, when the same experiments as the one reported in Fig. 1 were repeated in the presence of 4-dimethylaminopyridine (DMAP) as sacrificial electron donor the same kinetics was observed as those of the reaction in the absence of DMAP (**Fig. S6**), making the hypothesis of the CTA activation through an electron transfer pathway less probable. This conclusion is in line with the computational analysis in **Section 3.2**.

Moreover, it is worth noting that electron transfer requires very close proximity of the molecule and the surface whereas energy transfer can occur both in proximity up to several Angstrom far from the surface, meaning that, even when the fragments are not strongly interacting with the surface, an energy transfer can still occur which is relevant for the RAFT reaction in solution as discussed in **Sections 3.1** and **3.5**.

3.4. Computational investigation of CTAs' fragments adsorption

Once the CTA has been homolytically dissociated via energy transfer, the two radical fragments (R• and ZSS•) compete for the adsorption on the TiO_2 (1 0 1) anatase surface (Fig. 4**a** and Fig. 5**a**). The adsorption energy (E_{ads}) of the fragments on the TiO_2 (1 0 1) anatase surface model has been calculated as the difference between the total energy of the TiO_2/fragment system (E_{tot}) and the energy of the fragment (E_{fragm}) and that of the optimized TiO_2 surface slab model (E_{TiO2}):

$$E_{ads} = E_{tot} - \left(E_{fragm} + E_{TiO_2}\right) \quad (4)$$

The R• radical initiator of CPDB interacts with the TiO_2 surface

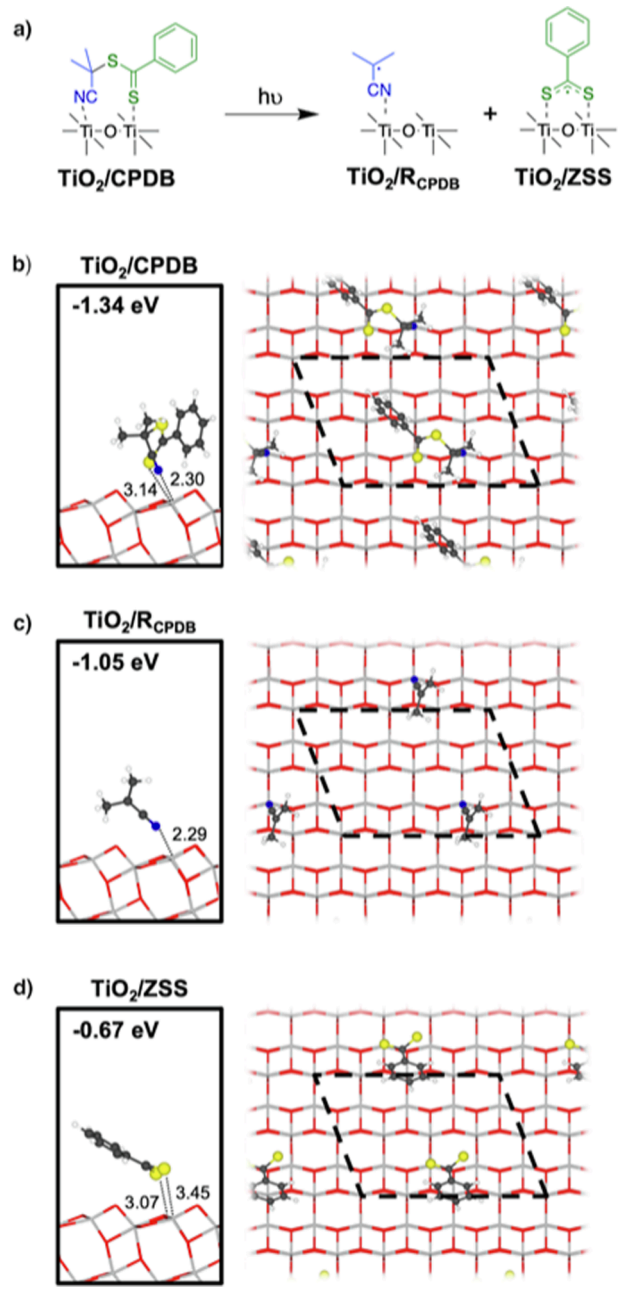

Fig. 4. Fragmentation of CPDB chain transfer agent on the TiO_2 surface. a) Schematic representation of the mechanism. Adsorption modes (side and top views) on the anatase (1 0 1) TiO_2 surface of b) CPDB; c) radical initiator generated from CPDB; and (d) ZSS radical. Adsorption energies are reported in eV. The overlying parallelogram in dashed line represents the supercell model used for the calculations. Relevant distances are reported in Å in the proximity of the dashed line.

through the CN group, whereas the ZSS• radical through the two S atoms on which the radical is found to be delocalized, as shown on the left side of Fig. 4**c and d**. The calculated adsorption energy is −1.05 eV and −0.67 eV for the radical initiator and the thiocarbonyl radical, respectively. Based on these values and on the fact that before dissociation both fragments were already in contact with the surface, as shown in Fig. 4**b**, we expect that after fragmentation both species will end up being adsorbed on the surface of TiO_2.

The R• radical initiator of CPADB interacts with the TiO_2 surface through both the carboxylic group and the CN group, as shown on the

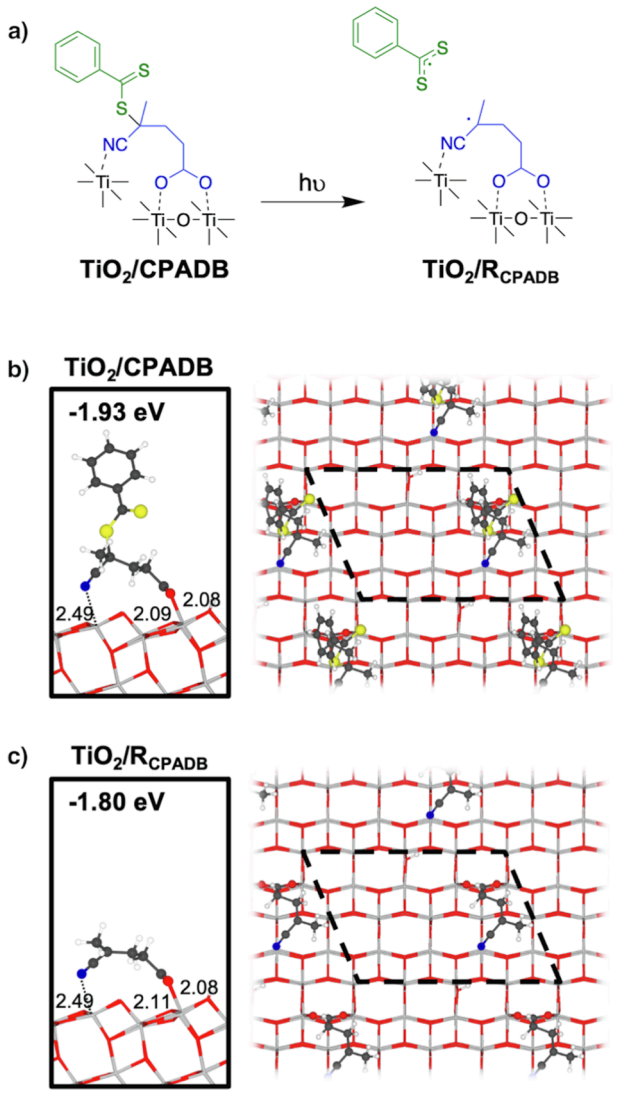

Fig. 5. Fragmentation of CPADB chain transfer agent on the TiO_2 surface. a) Schematic representation of the mechanism. Adsorption modes (side and top views) on the anatase (1 0 1) TiO_2 surface of b) CPADB; c) radical initiator generated from CPADB. Adsorption energies are reported in eV. The overlying parallelogram in dashed line represents the supercell model used for the calculations. Relevant distances are reported in Å in the proximity of the dashed line.

left side of Fig. 5**c**, in perfect analogy to the corresponding non-dissociated CTA, as shown in Fig. 5**b**. The carboxylic group strongly binds the surface in a dissociated bridging bidentate mode, with a calculated adsorption energy of −1.80 eV, which is almost three times that calculated for the ZSS fragment (-0.67 eV). Based on these values and on the fact that the thiocarbonyl portion in the non-dissociated CPADB chain transfer agent is not interacting with the surface (as shown on the left side of Fig. 5**b**), we expect that, after fragmentation, the anatase (1 0 1) surface of TiO_2 becomes prevalently covered by the radical initiator, with limited access to the surface by the ZSS fragment.

The lower probability for the thiocarbonyl radical generated from the CPADB to stably interact with the TiO_2 surface with respect to the ZSS radical generated from the CPDB, makes it more available in the DMF medium for the RAFT process, which is expected to accelerate the polymerization, thus explaining the different kinetics observed in **Section 3.1**. This analysis can also give a rational basis to the experimental data presented in **Section 3.5**, as it will be further discussed below.

To get a deeper insight into the electronic properties, we calculated the total (TDOS) and the projected density of states (PDOS) for the thiocarbonyl radical, which is the species that acts as a transfer agent for the polymerization process, adsorbed on the TiO_2 (1 0 1) anatase surface. Since the radical system is now a doublet spin state, we can see in the PDOS the loss of alignment of the spin α (up) and β (down) components (Fig. 6 top panel). Moreover, the plotted PDOS shows the presence of an empty molecular state localized just below the conduction band of the semiconductor. This state indicates that the system could easily take a photoexcited electron from the environment and thus evolve into a charged ZSS fragment.

The charged ZSS fragment interacts with the surface through the two sulfur atoms that bind on two different undercoordinated Ti_{5c} atoms. When the fragment is charged the interaction with the surface is stronger with respect to when it is in the radical form. This is shown not only by the geometry configuration which presents shorter S-Ti bonds (3.07 Å and 3.45 Å for the radical versus 2.66 Å and 2.66 Å for the charged), but also by the adsorption energy that is −1.51 eV for the charged thiocarbonyl (against −0.67 eV for the thiocarbonyl radical). From its PDOS analysis (Fig. 6 bottom panel), once more there are levels inside the band gap of the material which are occupied states coming from the charged moiety that reduce the gap between the highest occupied state and the lowest unoccupied state to 2.72 eV. These new states inside the band gap of TiO_2 correspond to π orbitals localized on both the S atoms of the thiocarbonyl, as shown in the plotted electronic density of Fig. 6. It is worth noting as the bottom of the conduction band of the system is still mainly composed of titanium atoms.

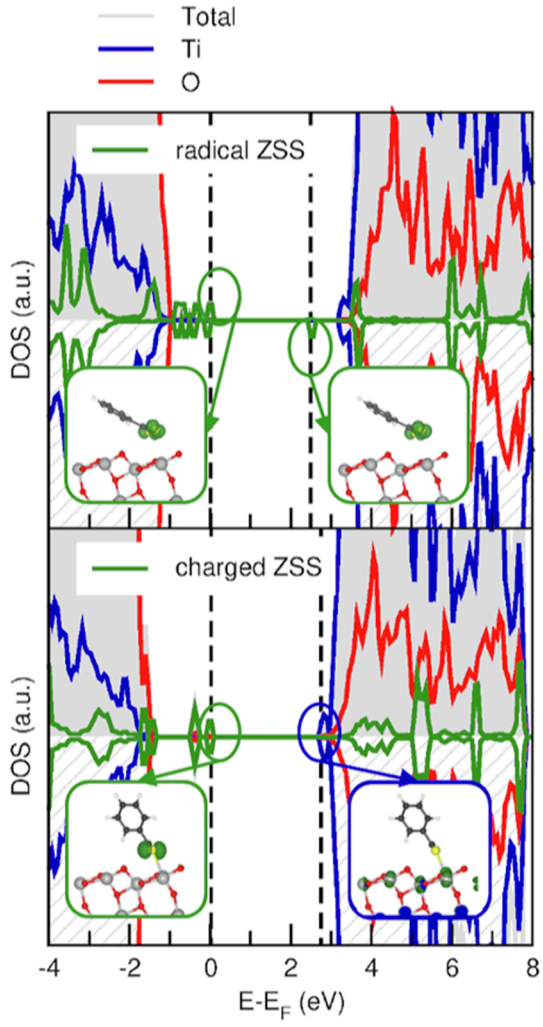

Fig. 6. TDOS and PDOS of the a) radical and b) charged ZSS adsorbed on the TiO_2 (1 0 1) anatase surface with both spin α (up) and β (down) components. On each panel are reported the plotted density of the highest occupied state and the lowest unoccupied state, and their position using dashed lines.

The high stability of the charged thiocarbonyl fragment with respect to its radical form suggests that even after homolytic fragmentation it could evolve into a charged moiety by easily taking a photoexcited electron.

3.5. Investigation of photocatalyst surface area dependency

As highlighted by the computational analysis, the titanium dioxide surface plays a crucial role in the initiation of the polymerization. In fact, PET-RAFT polymerization is expected to occur at the interface of the photocatalytic nanoparticles. Moreover, both the R• and ZSS• fragments of the CTAs have a certain affinity with the surface, giving rise to a competitive interaction that influences the polymerization outcomes.

Considering the importance of the surface area (A_{sup}) in heterogeneous catalysis, PET-RAFT polymerizations with the two CTAs were performed varying the A_{sup} of the PC. Since all polymerizations are performed in solution, the surface area of TiO_2 strongly depends on its agglomeration state. For this reason, in order to achieve different surface area values, maintaining the same photocatalyst, we have varied the solvent/monomer ratio. TiO_2 is better dispersed in a polar environment, thus a higher surface area was obtained when the amount of DMF was higher than the amount of MMA ($X_{DMF/MMA} = 0.71$). Moreover, even if increasing the concentration of TiO_2 nanoparticles causes aggregation phenomenon, higher surface area can still be reached. DLS analysis was exploited to obtain the hydrodynamic volume of TiO_2 aggregates in the dispersing polymerization media and the total surface area per millilitre of dispersion has been calculated using the following formula:

$$A_{sup/mL} = 4\pi R_H^2 * N_{part/mL} \quad (5)$$

where

$$N_{part/mL} = \frac{[TiO_2]}{\rho_{TiO_2} * 4/3\pi R_H^3} \quad (6)$$

Polymerization of PMMA was repeated changing the accessible surface area of TiO_2 by adapting the parameters of DMF/MMA ratio and of the PC concentration, as reported in Table 2. The obtained results are summarized in Fig. 7**a and 7b**.

In the case of CPDB, an increase in the TiO_2 surface area determines higher monomer conversion with an exponential trend. It is important to note that this increase cannot be attributed to the larger DMF/MMA ratio (Table 2) because a lower MMA concentration would on the contrary reduce the reaction rate according to the following kinetic equation of RAFT polymerization [1].

$$R_p(t) = k_p[M]\sqrt{\frac{fk_d[I]_0 e^{-k_d t}}{k_t}} \quad (7)$$

where R_p is the polymerization rate, k_p the propagation rate coefficient, $[M]$ the monomer concentration, f the initiator efficacy, k_d the decomposition rate coefficient of the initiator, $[I]_0$ the initial initiator concentration and k_t the termination rate coefficient.

These empirical results also confirm the hypothesis that the PET-RAFT mechanism occurs at the photocatalyst interface, since indeed when the TiO_2 surface area increases the photocatalytic activity increases as well, and the reaction is accelerated. At very low surface areas the increase in monomer conversion follows a linear trend, which deviates from linearity when the surface increases, reaching a plateau.

Various studies on Degussa P25 TiO_2 photocatalytic performance are available in the literature showing that high catalyst loading can reduce the photocatalytic performance rather than increasing it, and above certain concentrations, the increase in the turbidity of the dispersion

Table 2
PET-RAFT polymerization of PMMA at increasing TiO_2 concentration.

[TiO_2] (mg/mL)	$X_{(DMF/MMA)}$ [a]	R_H [b] (nm)	A_{sup}/mL (m^2/mL)	CPDB		CPADB	
				Entry	Conv % [c]	Entry	Conv % [c]
0.15	0.23	1099	9.31E-05	1	6.76	9	9.27
0.17	0.11	643	1.84E-04	2	10.25	10	18.38
0.17	0.07	435	2.82E-04	3	11.77	11	19.68
0.32	0.71	206	1.09E-03	4	13.85	12	16.03
0.48	0.71	159	2.13E-03	5	14.34	13	13.18
1.28	0.71	153	5.90E-03	6	22.46	14	23.55
1.92	0.71	166	8.14E-03	7	24.45	15	22.05
3.20	0.71	162	1.39E-02	8	26.61	16	19.02

[a] $\chi_{(DMF/MMA)}$ is the volume fraction of DMF in comparison with MMA.
[b] Hydrodynamic radius has been obtained by DLS measurement.
[c] Conversion has been calculated by NMR.

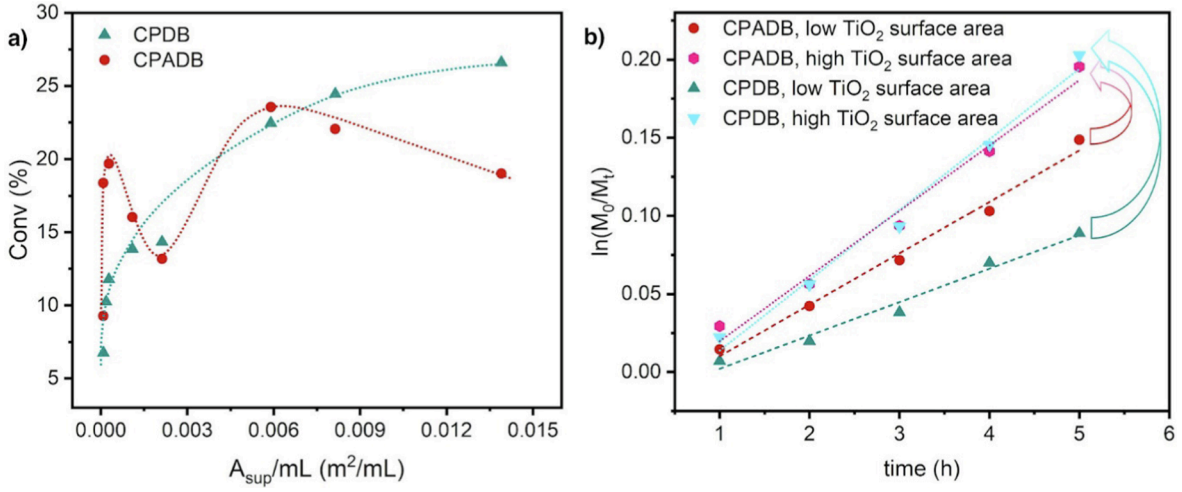

Fig. 7. a) Monomer conversion versus the calculated surface area of polymerization using CPDB (green triangle) and CPADB (red dots). Monomer conversion refers to polymer content in solution. b) Kinetic comparison of PMMA PET-RAFT polymerization using cpadb (red and pink dots) and CPDB (green and blue triangle) as CTAs under UV light irradiation with TiO_2 photocatalyst. Regarding the legend, CPADB low TiO_2 surface area refers to entry 9, CPADB high TiO_2 surface area refers to entry 13, CPDB low TiO_2 surface area refers to entry 1, CPDB high TiO_2 surface area refers to entry 5 from Table 2. The calculated error on x and y axes are reported in the SI (characterization techniques). (For interpretation of the references to color in this figure legend, the reader is referred to the web version of this article.)

reduces the light transmission [21,64]. This means that not all particles are available for photoexcitation, and they do not likely contribute to the catalytic activity.

On the contrary, the behavior of CPADB shows an unexpected trend. At a sufficiently low surface area (i.e < 0.003 m^2/mL) the monomer conversion reaches a maximum and then decreases. This trend can be connected to the mechanistic results from the computational study reported in the previous **Section 3.4**. In details, the faster reaction kinetics of CPADB can be associated with the low retention time of the thiocarbonyl portion of the CTA on the surface of titanium dioxide, due to the competitive surface adsorption of the carboxylic R-end functionality. This competition does not occur for CPDB, where no strong interaction of the R-group has been observed, thus explaining the different conversion rates of the two RAFT agents at low surface area values.

When the surface area of titanium dioxide increases, the ratio between the surface sites and the CPADB increases, resulting in an enhancement of the monomer conversion until it reaches a maximum. This maximum corresponds to the situation in which a wide portion of the surface is covered by the R-end functionality of the CTA and the thiocarbonyl fragment is not retained by the TiO_2. A further increase in the surface area and in the PC/CTA ratio causes an increase in the available surface sites for the thiocarbonyl radical interaction. The competitive interactions between the R-group and the dithioester radical become less relevant, until the kinetics of CPADB and CPDB become comparable (Samples 5 and 13 in Table 1). This mechanism is illustrated in Fig. 8.

Even at higher surface area values, as expected, the conversion drastically increases, but then slightly decreases again. This second drop regime can be explained by the fact that the data refer to the content of polymer in solution, thus it does not consider the amount of polymer grafted on titanium dioxide. TGA analysis demonstrates an increase in the amount of polymer chains grafted on TiO_2 in parallel with increasing surface area (**Fig. S7**).

3.6. *Going from UV to blue light by N-doping of TiO_2*

In the previous sections, we have focused our efforts on determining the photocatalytic role of TiO_2 in the PET-RAFT process, where titanium

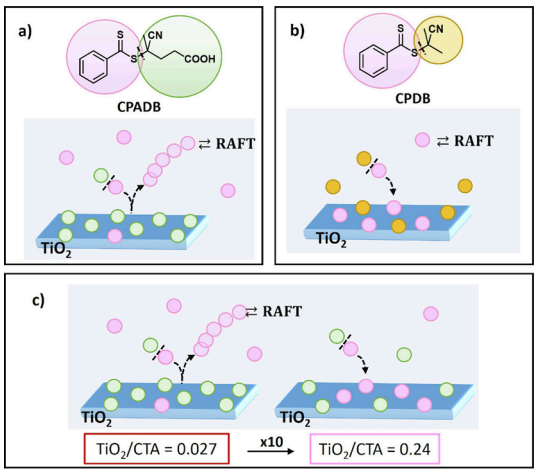

Fig. 8. Graphical sketch of the interactions of ZSS and R groups of a) CPADB and b) CPDB on TiO_2 surface. Figure c) represents the situation in which CPADB is used as CTA and the available surface area increases, while the amount of CTA decreases. On the left side it is represented entry 9 and on the right entry 13 (see Table 1).

dioxide can absorb only short-wavelength irradiation due to its wide band gap of 3.20 eV. However, UV-light is not the best option for PET-RAFT polymerization, due to the photolability of the C-S bond of dithiobenzoate CTAs, which brings to a quick loss of control, as shown from the control experiments reported in **Section 3.1**. For this reason, we decided to chemically shift the absorption of titanium dioxide in the visible light portion of the spectrum, with the aim to reduce or, possibly, avoid the CTA degradation and to achieve a higher control of the polymerization.

The adsorption of dyes on the surface is an easy methodology to modify TiO_2 absorption properties [31,32] but it would alter the surface properties and saturate available adsorption sites, therefore it has been excluded. We achieved absorption in the blue region of the electromagnetic spectrum (460 nm) by introducing nitrogen into the chemical structure of titanium dioxide [33] by an easy sol–gel methodology following a modified literature procedure [51].

The N-doped TiO_2 sample has been structurally characterized by XRD and Raman spectroscopy, which allowed to identify the co-existence of anatase and rutile phases (**Fig. S8**), with a mean crystallite size of 12.5 nm (**Fig. S9**). According to several studies reporting the effective inclusion of photoactive nitrogen in TiO_2 nanostructures, UV–vis diffuse reflectance spectrum of N-doped TiO_2 powder (**Fig. S10**) revealed the presence of an absorption tail in the sub-band gap region of titania, at λ above 400 nm, corroborating the successful shift of the photocatalyst absorption in the visible range.

X-Band Electron Paramagnetic Resonance (EPR) spectroscopy allowed the direct detection of N-based defects in the titania lattice. The spectrum of N-TiO_2 (Fig. 9**a**, bottom) is characterized by an orthorhombic signal with EPR parameters (i.e. *g*-values and hyperfine constants) consistent with those reported by Di Valentin et al. [65], Livraghi et al. [66,67], and Chiesa et al. [68], and assigned to nitric oxide (NO) species segregated in some lattice imperfection of the TiO_2 structure. Following the saturation behavior as a function of the microwaves power (Fig. 9**b**), the presence of a second and weak paramagnetic species has been unveiled, whose *g*-value and hyperfine coupling match those previously assigned to $NO^{2-\bullet}$ centers [68].

According to this attribution, the surface chemical composition and chemical states of N-doped TiO_2 analyzed by means of XPS (**Fig. S11**), revealed the presence of a single N species detectable at 399.5 eV, which is generally assigned to NO interstitial sites [69,70]. The surface N/Ti and N/O atomic ratios were also calculated and correspond to ~0.009.

These results confirm the successful doping of the titania structure with photoactive N-interstitial centers (Fig. 9**a**, top), which on one hand extends the absorption, but could also influence the photocatalytic activity. However, it is still not clear whether the effect is an enhancement of the charge separation, thus favoring electron transfer mechanisms [68,71], or a promotion of the charge-carrier recombination by the localized band gap states associated with nitrogen doping, thus inhibiting the electron transfer.

In this respect, some of us recently proved that nitrogen species in anatase TiO_2 NPs enhance the recombination of photogenerated charge carriers by photoluminescence (PL) spectroscopic measurements detecting a strong emission that has been assigned to a dopant-induced radiative deactivation of photoexcited states [57]. In heterogeneous photocatalysis, recombination often represents a detrimental phenomenon, which dissipates the energy absorbed after irradiation, suppressing the material photoactivity. However, this energy can, in principle, be absorbed by species that possess proper electronic features, fostering energy transfer mechanisms able to activate several important reactions [72].

Polymerization of PMMA with the newly synthesized N-doped TiO_2 nanoparticles as a photoredox catalyst under blue LED light (λ_{max} = 460 nm) has been carried out. CPADB has been selected as the chain transfer agent, according to previous works by Quiao et al. [73] and Boyer et al. [74] reporting that CPADB was largely inactive in promoting photoiniferter (PI)-RAFT of MA and MMA. CPADB has low absorption in the visible region of the electromagnetic spectrum, with a relative maximum of 510 nm [40]. Consequently, thiocarbonate chain transfer agents are usually preferred over dithiobenzoate for blue light PI-RAFT polymerization [75]. In addition, Konkolewicz et al. [76] show that electron-withdrawing groups decrease the efficiency of photoactivation. For these reasons, and because of the stronger absorption of N-TiO_2 at 460 nm, competition between PET-RAFT and PI-RAFT has been considered negligible in this scenario, and the PET-RAFT energy transfer pathway is expected to be the predominant mechanism.

As shown in Table 3**,** after 24 h, 43 % of conversion was reached and good control over the polymerization was obtained (Đ = 1.17) even at long irradiation time. The color of the dispersion did not change during the irradiation (Fig. 10**a**) and the CPADB signal can be observed in the aromatic region of the NMR spectra (Fig. 10**c**).

The overall results show a high degree of livingness. According to the EPR results, and the computational outcomes indicating that CPADB and CPDB chain transfer agents represent suitable species for energy transfer, the remarkable performance of N-doped TiO_2 in the polymerization

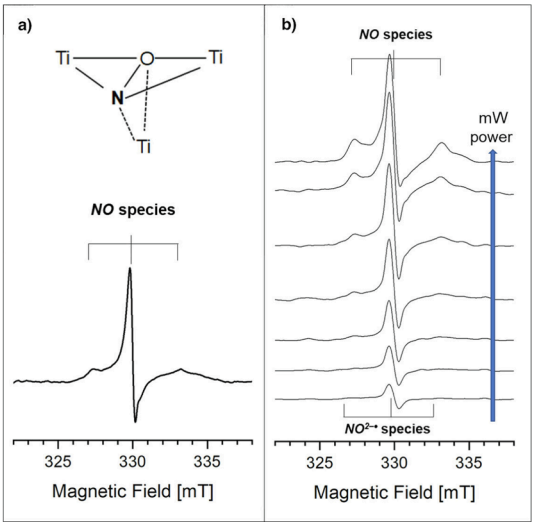

Fig. 9. a) Top, pictorial view of n interstitial center in N-TiO_2; bottom, EPR spectrum at 130 K in vacuo ($p < 10^{-5}$ mbar) of N-TiO_2 nanocrystals. b) Spectra of N-TiO_2 recorded at different mW power at 130 K in vacuo.

Table 3
PET-RAFT polymerization with N-TiO_2 photocatalyst under blue light for 24 h at room temperature.

Entry	Time (h)	[N-TiO_2] (mg/mL)	CTA	Conv % [a]	$M_{n,th}$ [b]	$M_{n,GPC}$ [c]	Đ [c]
17	24	0.48	CPADB	43.3	13 200	13 700	1.17

[a] Monomer conversion calculated with NMR analysis.
[b] Theoretical molecular weight ($M_{n,th}$) was calculated according to the formula $M_{n,th} = ([M]_0/[CTA]_0) \times MW^M \times \alpha + MW^{CTA}$, where $[M]_0$, $[CTA]_0$,MW^M, α, and MW^{CTA} correspond to initial monomer and CTA concentration, molar mass of monomer, conversion determined by ^1H NMR, and molar mass of CTA.
[c] $M_{n,GPC}$ and dispersity obtained by GPC measures.

of PMMA may find its origin in an energy-transfer-driven pathway promoted by the electronic structures of both the photocatalyst and CTA molecules adsorbed on the TiO_2 surface.

These very promising outcomes confirm that shifting toward less energetic light avoids CTA photodegradation and increases the livingness of the system even after 24 h under irradiation. This is the first report of PET-RAFT polymerization using the titanium dioxide photocatalyst under visible light.

4. Conclusions and future prospective

In this work, we have presented a comprehensive combined experimental and computational study of the photocatalytic mechanism of PET-RAFT polymerization using TiO_2 as the photocatalyst and CPADB and CPDB as the chain transfer agents.

Interaction between the two CTAs with the titanium dioxide surface was proved to be pivotal for the polymerization outcome both in terms of reaction kinetics and control. These interactions were confirmed both by experiments and by calculations. In particular, the carboxylic moiety of CPADB has excellent anchoring properties that influence the adsorption mode and increase the binding strength to the surface. In fact, experiments evidence that CPADB could be easily grafted on the TiO_2 surface in mild conditions. Moreover, calculations show that both CTAs are adsorbed on the TiO_2 surface with a calculated adsorption energy of −1.93 eV and −1.34 eV for CPADB and CPDB, respectively, meaning that the presence of the carboxylic functionality of CPDAB produces a slightly stronger interaction.

Investigation of the electronic properties of CPADB and CPDB adsorbed on the TiO_2 surface led to the conclusion that the initial step of fragmentation of the C-S bond of both CTAs is not possible through an electron transfer mechanism since the energy of the first empty state with the C-S anti-bonding character is too high. Whereas a photoinduced energy transfer mechanism is plausible because the wide band gap offers enough energy to homolytically break the C-S bond.

The hypothesis of an energy transfer mechanism is also supported by experiments with amines as sacrificial electron donors. The reaction kinetics in unaffected, which disproves an electron transfer mechanism confirming an energy transfer one.

Further computational investigation shows that once the CTA has been homolytically fragmented, the two radical species formed (ZSS• and R•) compete for the interaction with the TiO_2 surface. Based on the adsorption energy values and on the geometries of the fragments before and after dissociation, we observed a higher probability for the ZSS radical generated from the CPDB to stably interact with the TiO_2 surface with respect to the ZSS radical generated from the CPADB. This is due to the strong interaction of the carboxylic R-group of CPADB that reduces the available surface area and limits the retention of the ZSS fragment on the surface, making the latter more promptly available in the DMF medium for the RAFT process to occur, which is expected to accelerate the polymerization. The different behaviours observed experimentally for the two CTAs have been then justified based on the different competition for the surface interaction of the two fragments (R• and ZSS•).

This theoretical analysis has been further validated by additional experimental results for the polymerization at varying TiO_2 surface area.

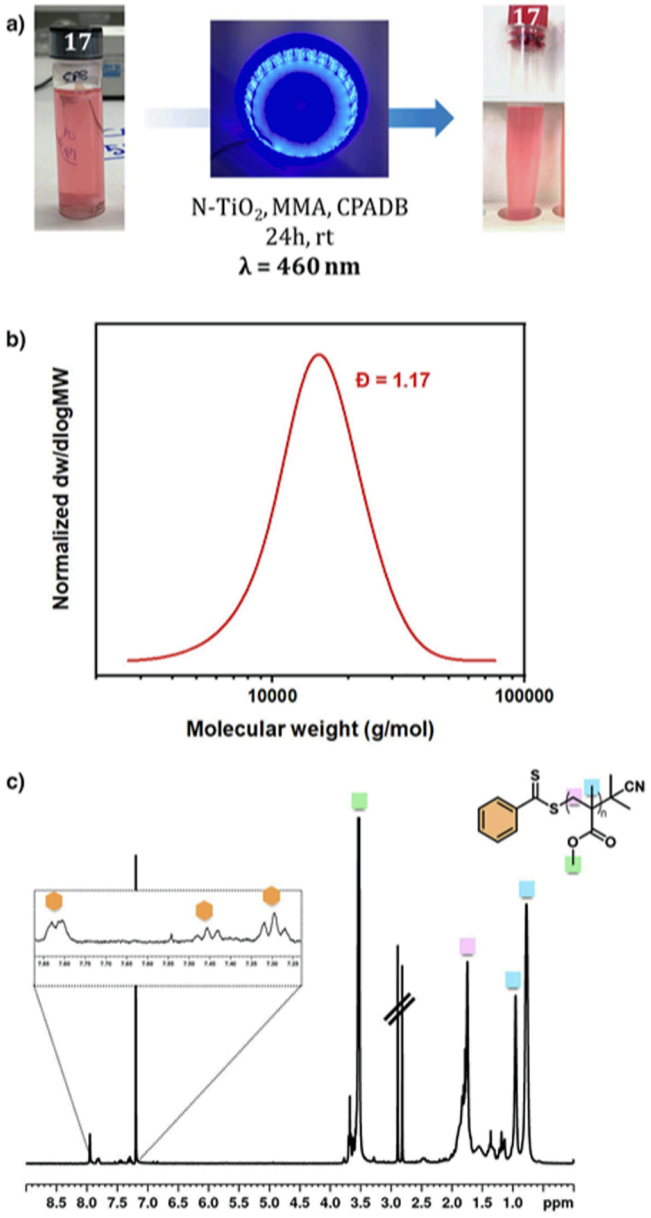

Fig. 10. a) PET-RAFT polymerization of MMA mediated by N-TiO_2 photocatalyst with CPADB under blue light at room temperature for 24 h. Good control over the polymerization was obtained with low dispersity and high-end group fidelity as displayed by the b) GPC traces and c) NMR spectrum of the polymer after purification. (For interpretation of the references to color in this figure legend, the reader is referred to the web version of this article.)

We showed that by sufficiently enlarging the TiO_2 surface area, the amount of CPADB R-group on the surface is no longer a limiting factor, thus the retention time of ZSS fragments of both CTAs becomes similar, and the kinetics of CPDB and CPADB overlap.

Finally, successful N-doping of titanium dioxide allowed to shift the polymerization under the less energetic blue light, achieving high control over the polymerization even after 24 h. This impressive result opens the possibility of a wider TiO_2 application in the controlled polymerization field.

This study helps to unravel some theoretical and experimental controversies about the different PET-RAFT mechanisms (photoinduced electron/energy transfer) using the TiO_2 catalyst and proves the key role played by the material's surface in the overall process.

Declaration of Competing Interest

The authors declare that they have no known competing financial interests or personal relationships that could have appeared to influence the work reported in this paper.

Data availability

Data will be made available on request.

Acknowledgments

The authors are grateful to Dr. Cinzia Cepek at CNR-IOM in Trieste for fruitful discussions and for her help with the XPS measurements. The project has received funding from the University of Milano Bicocca (Research Infrastructures Grant 2021).

Appendix A. Supplementary material

Supplementary data to this article can be found online at https://doi.org/10.1016/j.jcat.2023.07.015.

References

[1] A. Goto, T. Fukuda, Kinetics of living radical polymerization, Prog. Polym. Sci. 29 (2004) 329–385, https://doi.org/10.1016/j.progpolymsci.2004.01.002.
[2] J. Chiefari, Y.K.B. Chong, F. Ercole, J. Krstina, J. Jeffery, T.P.T. Le, R.T. A. Mayadunne, G.F. Meijs, C.L. Moad, G. Moad, E. Rizzardo, S.H. Thang, C. South, Living Free-Radical Polymerization by Reversible Addition - Fragmentation Chain Transfer: The RAFT Process, Macromolecules. 31 (1998) 5559–5562, https://doi.org/10.1021/ma9804951.
[3] K. Parkatzidis, H.S. Wang, N.P. Truong, A. Anastasaki, R. Developments, F. Challenges, in Controlled Radical Polymerization: A,, Update, Chem. 6 (2020) (2020) 1575–1588, https://doi.org/10.1016/j.chempr.2020.06.014.
[4] G. Moad, E. Rizzardo, S.H. Thang, Living radical polymerization by the RAFT process, Aust. J. Chem. 58 (2005) 379–410, https://doi.org/10.1071/CH05072.
[5] R. Whitfield, K. Parkatzidis, N.P. Truong, T. Junkers, A. Anastasaki, Tailoring Polymer Dispersity by RAFT Polymerization: A Versatile Approach, Chem. 6 (2020) 1340–1352, https://doi.org/10.1016/j.chempr.2020.04.020.
[6] V. Bellotti, K. Parkatzidis, H.S. Wang, N. De Alwis Watuthanthrige, M. Orfano, A. Monguzzi, N.P. Truong, R. Simonutti, A. Anastasaki, Light-accelerated depolymerization catalyzed by Eosin Y, Polym. Chem. 14 (2022) 253–258, https://doi.org/10.1039/d2py01383e.
[7] J.B. Young, J.I. Bowman, C.B. Eades, A.J. Wong, B.S. Sumerlin, Photoassisted Radical Depolymerization, ACS Macro Lett. 11 (2022) 1390–1395, https://doi.org/10.1021/acsmacrolett.2c00603.
[8] V. Bellotti, R. Simonutti, New light in polymer science: Photoinduced reversible addition-fragmentation chain transfer polymerization (PET-RAFT) as innovative strategy for the synthesis of advanced materials, Polymers (Basel). 13 (2021) 1119, https://doi.org/10.3390/polym13071119.
[9] J. Xu, K. Jung, A. Atme, S. Shanmugam, C. Boyer, A robust and versatile photoinduced living polymerization of conjugated and unconjugated monomers and its oxygen tolerance, J. Am. Chem. Soc. 136 (2014) 5508–5519, https://doi.org/10.1021/ja501745g.
[10] J. Xu, K. Jung, N.A. Corrigan, C. Boyer, Aqueous photoinduced living/controlled polymerization: Tailoring for bioconjugation, Chem. Sci. 5 (2014) 3568–3575, https://doi.org/10.1039/c4sc01309c.
[11] S. Shanmugam, J. Xu, C. Boyer, Exploiting Metalloporphyrins for Selective Living Radical Polymerization Tunable over Visible Wavelengths, J. Am. Chem. Soc. 137 (2015) 9174–9185, https://doi.org/10.1021/jacs.5b05274.
[12] S. Shanmugam, J. Xu, C. Boyer, Light-regulated polymerization under near-infrared/far-red irradiation catalyzed by bacteriochlorophyll a, Angew. Chemie - Int. Ed. 55 (2016) 1036–1040, https://doi.org/10.1002/anie.201510037.
[13] S. Shanmugam, J. Xu, C. Boyer, Utilizing the electron transfer mechanism of chlorophyll a under light for controlled radical polymerization, Chem. Sci. 6 (2015) 1341–1349, https://doi.org/10.1039/c4sc03342f.
[14] C.A. Figg, J.D. Hickman, G.M. Scheutz, S. Shanmugam, R.N. Carmean, B.S. Tucker, C. Boyer, B.S. Sumerlin, Color-Coding Visible Light Polymerizations to Elucidate the Activation of Trithiocarbonates Using Eosin y, Macromolecules. 51 (2018) 1370–1376, https://doi.org/10.1021/acs.macromol.7b02533.
[15] J. Xu, S. Shanmugam, C. Boyer, Organic Electron Donor-Acceptor Photoredox Catalysts: Enhanced Catalytic Efficiency toward Controlled Radical Polymerization, ACS Macro Lett. 4 (2015) 926–932, https://doi.org/10.1021/acsmacrolett.5b00460.
[16] Y. Zhu, Y. Liu, K.A. Miller, H. Zhu, E. Egap, Lead Halide Perovskite Nanocrystals as Photocatalysts for PET-RAFT Polymerization under Visible and Near-Infrared Irradiation, ACS Macro Lett. 9 (2020) 725–730, https://doi.org/10.1021/acsmacrolett.0c00232.
[17] Y. Zhu, E. Egap, PET-RAFT polymerization catalyzed by cadmium selenide quantum dots (qds): Grafting-from qds photocatalysts to make polymer nanocomposites, Polym. Chem. 11 (2020) 1018–1024. Doi:10.1039/c9py01604j.
[18] Y. Liang, H. Ma, W. Zhang, Z. Cui, P. Fu, M. Liu, X. Qiao, X. Pang, Size effect of semiconductor quantum dots as photocatalysts for PET-RAFT polymerization, Polym. Chem. 11 (2020) 4961–4967, https://doi.org/10.1039/D0PY00588F.
[19] Q. Fu, Q. Ruan, T.G. McKenzie, A. Reyhani, J. Tang, G.G. Qiao, Development of a Robust PET-RAFT Polymerization Using Graphitic Carbon Nitride (g-C3N4), Macromolecules. 50 (2017) 7509–7516, https://doi.org/10.1021/acs.macromol.7b01651.
[20] G.G. Rao, NEWER ASPECTS OF NITRIFICATION: I, Soil Sci. 38 (1934) 143–160. https://journals.lww.com/soilsci/Fulltext/1934/08000/NEWER_ASPECTS_OF_NITRIFICATION_I.6.aspx.
[21] A. Sebti, H. Lebik, F. Madjene, B. Boutra, A review: nano science for environmental remediation, Int. J. Sci. Res. Manag. Stud. 1 (2018) 242–247.
[22] J. Ferber, J. Luther, Modeling of photovoltage and photocurrent in dye-sensitized titanium dioxide solar cells, J. Phys. Chem. B. 105 (2002) 4895–4903, https://doi.org/10.1021/jp002928j.
[23] A. Miyoshi, S. Nishioka, K. Maeda, Water Splitting on Rutile TiO_2-Based Photocatalysts, Chem. - A Eur. J. 24 (2018) 18204–18219, https://doi.org/10.1002/chem.201800799.
[24] J. Schneider, M. Matsuoka, M. Takeuchi, J. Zhang, Y. Horiuchi, M. Anpo, D. W. Bahnemann, Understanding TiO_2 Photocatalysis Mechanisms and Materials, Chem. Rev. 114 (2014) 9919–9986, https://doi.org/10.1021/cr5001892.
[25] K. Nakata, A. Fujishima, TiO_2 photocatalysis: Design and applications, J. Photochem. Photobiol. C Photochem. Rev. 13 (2012) 169–189, https://doi.org/10.1016/j.jphotochemrev.2012.06.001.
[26] Q. Guo, C. Zhou, Z. Ma, X. Yang, Fundamentals of TiO_2 Photocatalysis: Concepts, Mechanisms, and Challenges, Adv. Mater. 31 (2019), https://doi.org/10.1002/adma.201901997.
[27] M.H.N. Assadi, D.A.H. Hanaor, The effects of copper doping on photocatalytic activity at (101) planes of anatase TiO2: A theoretical study, Appl. Surf. Sci. 387 (2016) 682–689, https://doi.org/10.1016/j.apsusc.2016.06.178.
[28] P. Niu, G. Wu, P. Chen, H. Zheng, Q. Cao, H. Jiang, Optimization of Boron Doped TiO_2 as an Efficient Visible Light-Driven Photocatalyst for Organic Dye Degradation With High Reusability, Front. Chem. 8 (2020) 1–8, https://doi.org/10.3389/fchem.2020.00172.
[29] P.S. Basavarajappa, S.B. Patil, N. Ganganagappa, K.R. Reddy, A.V. Raghu, C. V. Reddy, Recent progress in metal-doped TiO_2, non-metal doped/codoped TiO_2 and TiO_2 nanostructured hybrids for enhanced photocatalysis, Int. J. Hydrogen Energy. 45 (2020) 7764–7778, https://doi.org/10.1016/j.ijhydene.2019.07.241.
[30] A. Khlyustova, N. Sirotkin, T. Kusova, A. Kraev, V. Titov, A. Agafonov, Doped TiO_2: The effect of doping elements on photocatalytic activity, Mater. Adv. 1 (2020) 1193–1201, https://doi.org/10.1039/d0ma00171f.
[31] W.M. Campbell, A.K. Burrell, D.L. Officer, K.W. Jolley, Porphyrins as light harvesters in the dye-sensitised TiO_2 solar cell, Coord. Chem. Rev. 248 (2004) 1363–1379, https://doi.org/10.1016/j.ccr.2004.01.007.
[32] A. Andrzejewska, A. Krysztafkiewicz, T. Jesionowski, Adsorption of organic dyes on the aminosilane modified TiO_2 surface, Dye. Pigment. 62 (2004) 121–130, https://doi.org/10.1016/j.dyepig.2003.11.014.
[33] R. Asahi, T. Morikawa, T. Ohwaki, K. Aoki, Y. Taga, Visible-light photocatalysis in nitrogen-doped titanium oxides, Science. 293 (2001) 269–271, https://doi.org/10.1126/science.1061051.
[34] H. Irie, Y. Watanabe, K. Hashimoto, Nitrogen-concentration dependence on photocatalytic activity of $TiO_{2-x}N_x$ powders, J. Phys. Chem. B. 107 (2003) 5483–5486, https://doi.org/10.1021/jp030133h.
[35] J. Wang, D.N. Tafen, J.P. Lewis, Z. Hong, A. Manivannan, M. Zhi, M. Li, N. Wu, Origin of photocatalytic activity of Nitrogen-doped TiO_2 nanobelts, J. Am. Chem. Soc. 131 (2009) 12290–12297, https://doi.org/10.1021/ja903781h.
[36] X. Wang, S.O. Pehkonen, J. Rämö, M. Väänänen, J.G. Highfield, K. Laasonen, Experimental and computational studies of nitrogen doped Degussa P25 TiO_2: Application to visible-light driven photo-oxidation of As(III), Catal, Sci. Technol. 2 (2012) 784–793, https://doi.org/10.1039/c2cy00486k.
[37] X. Fang, Z. Zhang, Q. Chen, H. Ji, X. Gao, Dependence of nitrogen doping on TiO_2 precursor annealed under NH3 flow, J. Solid State Chem. 180 (2007) 1325–1332, https://doi.org/10.1016/j.jssc.2007.02.010.
[38] C. Shifu, C. Lei, G. Shen, C. Gengyu, The preparation of nitrogen-doped photocatalyst $TiO_{2-x}N_x$ by ball milling, Chem. Phys. Lett. 413 (2005) 404–409, https://doi.org/10.1016/j.cplett.2005.08.038.
[39] B.F. Cheng, L.H. Wang, Y.Z. You, Photoinduced electron transfer-reversible addition-fragmentation chain transfer (PET-RAFT) polymerization using titanium dioxide, Macromol. Res. 24 (2016) 811–815, https://doi.org/10.1007/s13233-016-4106-5.
[40] M. Hartlieb, Photo-Iniferter RAFT Polymerization, Macromol. Rapid Commun. 43 (2022), https://doi.org/10.1002/marc.202100514.
[41] J.F. Quinn, L. Barner, C. Barner-Kowollik, E. Rizzardo, T.P. Davis, Reversible Addition−Fragmentation Chain Transfer Polymerization Initiated with Ultraviolet Radiation, Macromolecules. 35 (2002) 7620–7627, https://doi.org/10.1021/ma0204296.
[42] R.N. Carmean, C.A. Figg, G.M. Scheutz, T. Kubo, B.S. Sumerlin, Catalyst-Free Photoinduced End-Group Removal of Thiocarbonylthio Functionality, ACS Macro Lett. 6 (2017) 185–189, https://doi.org/10.1021/acsmacrolett.7b00038.
[43] M.D. Thum, S. Wolf, D.E. Falvey, State-Dependent Photochemical and Photophysical Behavior of Dithiolate Ester and Trithiocarbonate Reversible Addition-Fragmentation Chain Transfer Polymerization Agents, J. Phys. Chem. A. 124 (2020) 4211–4222, https://doi.org/10.1021/acs.jpca.0c02678.

[44] J. Phommalysack-Lovan, Y. Chu, C. Boyer, J. Xu, PET-RAFT polymerisation: Towards green and precision polymer manufacturing, Chem. Commun. 54 (2018) 6591–6606, https://doi.org/10.1039/c8cc02783h.
[45] N. Corrigan, S. Shanmugam, J. Xu, C. Boyer, Photocatalysis in organic and polymer synthesis, Chem. Soc. Rev. 45 (2016) 6165–6212, https://doi.org/10.1039/c6cs00185h.
[46] D.J. Keddie, G. Moad, E. Rizzardo, S.H. Thang, RAFT agent design and synthesis, Macromolecules. 45 (2012) 5321–5342, https://doi.org/10.1021/ma300410v.
[47] S. Perrier, 50th Anniversary Perspective: RAFT Polymerization - A User Guide, Macromolecules. 50 (2017) 7433–7447, https://doi.org/10.1021/acs.macromol.7b00767.
[48] B. Ohtani, O.O. Prieto-Mahaney, D. Li, R. Abe, What is Degussa (Evonic) P25? Crystalline composition analysis, reconstruction from isolated pure particles and photocatalytic activity test, J. Photochem. Photobiol. A Chem. 216 (2010) 179–182, https://doi.org/10.1016/j.jphotochem.2010.07.024.
[49] S. Matsumura, A.R. Hlil, C. Lepiller, J. Gaudet, D. Guay, Z. Shi, S. Holdcroft, A. S. Hay, Stability and Utility of Pyridyl Disulfide Functionality in RAFT and Conventional Radical Polymerizations, J. Polym. Sci. Part A Polym. Chem. 46 (2008) 7207–7224, https://doi.org/10.1002/pola.
[50] S.H. Thang, B.Y.K. Chong, R.T.A. Mayadunne, G. Moad, E. Rizzardo, A novel synthesis of functional dithioesters, dithiocarbamates, xanthates and trithiocarbonates, Tetrahedron Lett. 40 (1999) 2435–2438, https://doi.org/10.1016/S0040-4039(99)00177-X.
[51] S.J. Bu, Z.G. Jin, X.X. Liu, L.R. Yang, Z.J. Cheng, Synthesis of TiO_2 porous thin films by polyethylene glycol templating and chemistry of the process, J. Eur. Ceram. Soc. 25 (2005) 673–679, https://doi.org/10.1016/j.jeurceramsoc.2003.12.025.
[52] S. Landi, I.R. Segundo, E. Freitas, M. Vasilevskiy, J. Carneiro, C.J. Tavares, Use and misuse of the Kubelka-Munk function to obtain the band gap energy from diffuse reflectance measurements, Solid State Commun. 341 (2022) 1–7, https://doi.org/10.1016/j.ssc.2021.114573.
[53] R. Dovesi, V. R. Saunders, C. Roetti, R. Orlando, C. M. Zicovich-Wilson, F. Pascale, B. Civalleri, K. Doll, N. M. Harrison, I. J. Bush, P. D'Arco, M. Llunell, M. Causà, Y. Noël, L. Maschio, A. Erba, M. Rerat, S. Casassa, CRYSTAL17 User's Manual (University of Torino, Torino, 2017).
[54] A.D. Becke, A new mixing of Hartree-Fock and local density-functional theories, J. Chem. Phys. 98 (1993) 1372–1377, https://doi.org/10.1063/1.464304.
[55] S. Grimme, Semiempirical GGA-type density functional constructed with a long-range dispersion correction, J. Comput. Chem. 27 (2006) 1787–1799, https://doi.org/10.1002/jcc.20495.
[56] B. Civalleri, C.M. Zicovich-Wilson, L. Valenzano, P. Ugliengo, B3LYP augmented with an empirical dispersion term (B3LYP-D*) as applied to molecular crystals, CrystEngComm. 10 (2008) 405–410, https://doi.org/10.1039/B715018K.
[57] C. Deiana, E. Fois, S. Coluccia, G. Martra, Surface structure of TiO_2 P25 nanoparticles: Infrared study of hydroxy groups on coordinative defect sites, J. Phys. Chem. C. 114 (2010) 21531–21538, https://doi.org/10.1021/jp107671k.
[58] M. Tawfilas, M. Mauri, L. De Trizio, R. Lorenzi, R. Simonutti, Surface Characterization of TiO_2 Polymorphic Nanocrystals through ^{1}H-TD-NMR, Langmuir. 34 (2018) 9460–9469, https://doi.org/10.1021/acs.langmuir.8b01216.
[59] J.F. Quinn, E. Rizzardo, L. Barner, C. Barner-Kowollik, T.P. Davis, Reversible addition-fragmentation chain transfer polymerization initiated with ultraviolet and γ radiation: A comparison, Am. Chem. Soc. Polym. Prepr. Div. Polym. Chem. 43 (2002) 319–320.
[60] D. Selli, M. Tawfilas, M. Mauri, R. Simonutti, C. Di Valentin, Optimizing PEGylation of TiO_2 Nanocrystals through a Combined Experimental and Computational Study, Chem. Mater. 31 (2019) 7531–7546, https://doi.org/10.1021/acs.chemmater.9b02329.
[61] K.L. Materna, R.H. Crabtree, G.W. Brudvig, Anchoring groups for photocatalytic water oxidation on metal oxide surfaces, Chem. Soc. Rev. 46 (2017) 6099–6110, https://doi.org/10.1039/c7cs00314e.
[62] R. Luschtinetz, S. Gemming, G. Seifert, Anchoring functional molecules on TiO_2 surfaces: A comparison between the carboxylic and the phosphonic acid group, Eur. Phys. J. Plus. 126 (2011) 1–13, https://doi.org/10.1140/epjp/i2011-11098-4.
[63] B. Nomeir, O. Fabre, K. Ferji, Effect of Tertiary Amines on the Photoinduced Electron Transfer-Reversible Addition-Fragmentation Chain Transfer (PET-RAFT) Polymerization, Macromolecules. 52 (2019) 6898–6903, https://doi.org/10.1021/acs.macromol.9b01493.
[64] A. Das, M. Patra, R.R. Wary, P. Gupta, R.G. Nair, Photocatalytic performance analysis of Degussa P25 under various laboratory conditions, IOP Conf. Ser. Mater. Sci. Eng. 377 (2018), https://doi.org/10.1088/1757-899X/377/1/012101.
[65] C. Di Valentin, G. Pacchioni, A. Selloni, S. Livraghi, E. Giamello, Characterization of paramagnetic species in N-doped TiO_2 powders by EPR spectroscopy and DFT calculations, J. Phys. Chem. B. 109 (2005) 11414–11419, https://doi.org/10.1021/jp051756t.
[66] S. Livraghi, A. Votta, M.C. Paganini, E. Giamello, The nature of paramagnetic species in nitrogen doped TiO_2 active in visible light photocatalysis, Chem. Commun. (2005) 498–500, https://doi.org/10.1039/b413548b.
[67] S. Livraghi, M.C. Paganini, E. Giamello, A. Selloni, C. Di Valentin, G. Pacchioni, Origin of Photoactivity of Nitrogen-Doped Titanium Dioxide under Visible Light, J. Am. Chem. Soc. 128 (2006) 15666–15671, https://doi.org/10.1021/ja064164c.
[68] M. Chiesa, S. Livraghi, M.C. Paganini, E. Salvadori, E. Giamello, Nitrogen-doped semiconducting oxides. Implications on photochemical, photocatalytic and electronic properties derived from EPR spectroscopy, Chem. Sci. 11 (2020) 6623–6641, https://doi.org/10.1039/d0sc02876b.
[69] Y. Wang, C. Feng, M. Zhang, J. Yang, Z. Zhang, Enhanced visible light photocatalytic activity of N-doped TiO_2 in relation to single-electron-trapped oxygen vacancy and doped-nitrogen, Appl. Catal. B Environ. 100 (2010) 84–90, https://doi.org/10.1016/j.apcatb.2010.07.015.
[70] C. Di Valentin, E. Finazzi, G. Pacchioni, A. Selloni, S. Livraghi, M.C. Paganini, E. Giamello, N-doped TiO_2: Theory and experiment, Chem. Phys. 339 (2007) 44–56, https://doi.org/10.1016/j.chemphys.2007.07.020.
[71] G. Barolo, S. Livraghi, M. Chiesa, M.C. Paganini, E. Giamello, Mechanism of the photoactivity under visible light of N-doped titanium dioxide. Charge carriers migration in irradiated N-TiO_2 investigated by electron paramagnetic resonance, J. Phys. Chem. C. 116 (2012) 20887–20894. http://doi.org/10.1021/jp306123d.
[72] L. Schumacher, R. Marschall, Recent Advances in Semiconductor Heterojunctions and Z-Schemes for Photocatalytic Hydrogen Generation, Top. Curr. Chem. 380 (2022) 1–42, https://doi.org/10.1007/s41061-022-00406-5.
[73] T.G. McKenzie, L.P.M. Da Costa, Q. Fu, D.E. Dunstan, G.G. Qiao, Investigation into the photolytic stability of RAFT agents and the implications for photopolymerization reactions, Polym. Chem. 7 (2016) 4246–4253, https://doi.org/10.1039/c6py00808a.
[74] J. Xu, S. Shanmugam, N.A. Corrigan, C. Boyer, Catalyst-Free Visible Light-Induced RAFT Photopolymerization, in, Control. Radic. Polym. Mech. (2015) 247–267, https://doi.org/10.1021/bk-2015-1187.ch013.
[75] T.G. McKenzie, Q. Fu, E.H.H. Wong, D.E. Dunstan, G.G. Qiao, Visible Light Mediated Controlled Radical Polymerization in the Absence of Exogenous Radical Sources or Catalysts, Macromolecules. 48 (2015) 3864–3872, https://doi.org/10.1021/acs.macromol.5b00965.
[76] M.L. Allegrezza, N. De Alwis Watuthanthrige, Y. Wang, G.A. Garcia, H. Ren, D. Konkolewicz, Substituent effects in iniferter photopolymerization: Can bond homolysis be enhanced by electronics?, Polym. Chem. 11 (2020) 6129–6133. http://doi.org/10.1039/d0py01086c.